Use of a microscope stage-mounted Nickel-63 microirradiator for real-time observation of the DNA double-strand break response

Zhen Cao[1,2], Wendy W. Kuhne[1,3], Jennifer Steeb[4], Mark A. Merkley[1], Yunfeng Zhou[2], Jiri Janata[4] and William S. Dynan[1,*]

[1]Institute of Molecular Medicine and Genetics, Medical College of Georgia, Augusta, Georgia, USA, [2]Department of Chemotherapy and Radiation Oncology, Zhongnan Hospital, Wuhan University, Wuhan, Hubei 430071, PRC, [3]Savannah River National Laboratory, Savannah River Site, Aiken SC 29808 and [4]Department of Chemistry and Biochemistry, Georgia Institute of Technology, 901 Atlantic Drive, Atlanta, GA 30332, USA

ABSTRACT

Eukaryotic cells begin to assemble discrete, nucleoplasmic repair foci within seconds after the onset of exposure to ionizing radiation. Real-time imaging of this assembly has the potential to further our understanding of the effects of medical and environmental radiation exposure. Here, we describe a microirradiation system for targeted delivery of ionizing radiation to individual cells without the need for specialized facilities. The system consists of a 25-micron diameter electroplated Nickel-63 electrode, enveloped in a glass capillary and mounted in a micromanipulator. Because of the low energy of the beta radiation and the minute total amount of isotope present on the tip, the device can be safely handled with minimum precautions. We demonstrate the use of this system for tracking assembly of individual repair foci in real time in live U2OS human osteosarcoma cells. Results indicate that there is a subset of foci that appear and disappear rapidly, before a plateau level is reached ~30 min post-exposure. This subset of foci would not have been evident without real-time observation. The development of a microirradiation system that is compatible with a standard biomedical laboratory expands the potential for real-time investigation of the biological effects of ionizing radiation.

INTRODUCTION

Ionizing radiation affects living tissue in a unique way, by depositing energy along discrete, nanometer-scale tracks. When a track intersects DNA, damage can occur on both DNA strands simultaneously, leading to an outright chromosome break. Even one such break can cause chronic genetic instability or cancer-associated gene rearrangements. It is thus not surprising that ionizing radiation evokes complex biological defense and repair mechanisms. A central aspect of the radiation response is the self-assembly of nucleoplasmic repair foci, which is characterized by specific histone modifications, accumulation of DNA damage sensing and signal transduction proteins, and assembly of the DNA repair machine proper from pre-existing components. Repair foci begin to appear shortly after irradiation and resolve over the course of several hours (1,2)

Conventional methods for evoking this radiation response require placing cells or tissues in the proximity of a radiation source. These 'off-line' methods require physical transfer of samples from the irradiator to a microscope stage for observation, which precludes observation of early-stage assembly of repair foci in real time. In addition, one of the most common methods for laboratory irradiation requires a high-activity $^{137}CsCl_2$ source. These sources face increasing restrictions because they are perceived as threat to public health and safety in the event of an accident or attack (3). An inexpensive replacement technology using smaller amounts of isotope would address this concern.

One approach to address the shortcoming of conventional irradiation methods is to position a small radioisotope source in proximity to the sample on a microscope stage. One of the first examples of this approach was the use of a polonium-coated tungsten microneedle to deliver α particles to living cells (4). Recently, Steeb et al. (5) described an updated version of the microirradiator concept based on the deposition of isotopes by electroplating on a microelectrode enveloped by a glass

capillary. Importantly, the diameter of the microelectrode is on the same order as the size of a mammalian cell. Concentrated deposition of isotope within this small area allows for a high local radiation flux (10^6–10^9 Bq/cm^2) using subnanogram amounts of isotope. In addition, the electroplated surface can be recessed within the capillary, which allows the glass walls to act as a collimator for the beam (5). The concept was implemented using ^{63}Ni, a long-lived, low-energy β particle emitter. The maximum range of the emissions is only ∼60 μm in water or tissue, which allows the user to handle the device without special radiological precautions.

Here, we describe the first use of the ^{63}Ni microirradiator in a biological application. We mounted the device in a micromanipulator on the stage of a deconvolution microscope and used it to irradiate cultured human cells. Cells were transfected with expression constructs for fluorescently-tagged 53BP1, a widely used marker for DNA double-strand break repair foci [reviewed in (6,7)]. We collected real-time image data, which enabled quantitative characterization of the appearance, disappearance and motion of these foci. Initial studies suggest heterogeneous rates of formation and resolution, which could not have been observed using a conventional off-line radiation source.

MATERIALS AND METHODS

Microirradiator

The microirradiator was fabricated as described (5) with modifications as indicated below. ^{63}Ni is a low-energy β particle emitter (maximum energy 67 keV, average energy 17 keV) with a 100-year half life. The maximum range of the β particle emission in water is 60 μm (average range, 30 μm). A 25-μm Pt wire was threaded through a 0.5-cm bore diameter borosilicate glass capillary, which was flame-sealed and pulled in a glass electrode pulling apparatus at 800°C with a pull length of 3 cm. The end of the pulled Pt wire in glass was polished to produce a smooth disk. After cleaning, the electrode was electrochemically plated using a 50 mCi ^{63}NiCl$_2$ (1.6×10^{13} Bq/g) source (NRD LLC, Grand Island, NY, USA). This source was transformed into a pseudo Watts bath with the addition of NiSO$_4$ and H$_3$BO$_4$ for optimum Ni deposition. The Pt surface was deposited and monitored by constant potential (−0.75 V) until ample charge was passed (10^{-4} C) to indicate ^{63}Ni had plated the surface, extending slightly past the capillary. After ^{63}Ni deposition, a micron layer of Poly(3,4-ethylenedioxythiophene) (PEDOT) was deposited to ensure Ni did not interact with the cellular medium. A 0.1-mM solution of PEDOT was dissolved in 1 mM tetraethylammonium perchlorate in acetonitrile for 20 s at 0.25 V. Total activity of the microirradiator was 2000 Bq, as measured by liquid scintillation counting. The microirradiator was rinsed after each use and stored in a detergent solution.

Reporter plasmid

A PCR-XL-TOPO vector containing the human full-length 53BP1 open reading frame (ORF; locus accession number BC112161) was purchased from Open Biosystems (Huntsville, AL, USA). It was digested with KpnI and XhoI to release the 53BP1 ORF together with upstream and downstream untranslated regions (UTRs). The recipient vector, pENTR/D-TOPO (Invitrogen, Carlsbad, CA, USA) was first modified by insertion of an XhoI/KpnI polylinker and the 53BP1-encoding fragment was inserted between these two sites. To delete unwanted 5′-UTR sequences, a 520 nt N-terminal segment of the 53BP1 ORF was amplified using primers d(GGCG CTCGAGATGGACCCTACTGGAAGT) and d(GGCG CATATGGCACAGTATTTTCC), digested with XhoI and NdeI to create cohesive ends, and substituted for the corresponding XhoI–NdeI fragment in the natural cDNA, resulting in the promoterless pENTR/53BP1 vector. To insert an N-terminal fluorescent tag, the EYFP coding sequence was amplified, together with flanking Kozak consequence sequence, using primers d(GGCGGCGGCCGCGCCACCATGGTGAGCAAGG GCGAGG) and d(GCGCTCGAGCTTGTACAGCTCG TCCATGC). The product was cleaved with NotI and XhoI and inserted between the NotI and XhoI sites of pENTR/53BP1, upstream of and in frame with the 53BP1 ORF. The resulting construct was transferred using phage lambda recombinase into pcDNA-DEST40 (Invitrogen) for mammalian expression under the control of the CMV promoter/enhancer. The full sequence of the expression construct is provided in Supplementary Data.

Cells and electroporation conditions

U2OS 2-6-3 cells (8) were maintained in high glucose DMEM supplemented with GlutaMAX-1 (Invitrogen), 10% fetal bovine serum, 100 U/ml penicillin, 100 μg/ml streptomycin and 0.25 μg/ml Amphotericin B. Electroporation was performed using 3 μg of plasmid DNA and 40 μg of sheared salmon sperm DNA carrier (Ambion, Austin, TX, USA) using a Gene Pulser II (BioRad, Hercules, CA, USA). Electroporation was performed in a 0.4-cm cuvette containing 120 μl of culture medium, with settings of 170 V and 975 μF, resulting in a 60–90 ms time constant. Following electroporation, cells were seeded into glass bottom culture dishes (MatTek, Ashland, MA, USA) and incubated at 37°C to allow protein expression. Irradiation and imaging were performed 24–48 h post-electroporation.

Conventional γ irradiation and cell imaging

Cells were electroporated with plasmids encoding EYFP-53BP1 and H2B-diHcRed, a nuclear marker (9). Cells were irradiated using a self-contained ^{137}Cs irradiator (Gammacell 40 Exactor, MDS Nordion, Ottawa, ON, Canada) at a dose rate of 0.84 Gy/min, then transferred to the WeatherStation environmental chamber of an Applied Precision Deltavision microscope, where incubation was continued at 37°C in a humidified, 5% CO$_2$ atmosphere. Live cell images were collected using a 60X Plan Achro oil objective beginning 25–30 min post-irradiation. Filter sets were as follows: EYFP, 500 nm excitation/535 nm emission; diHcRed, 572 nm

excitation/632 nm emission. Z stacks of 15–24 images were collected using a 0.4-μm step size and deconvoluted using softWoRx software. Projection images were prepared and nuclear foci were scored manually. Analysis was restricted to cells that were positive for both EYFP and the diHcRed nuclear marker (>80% of the population). To determine the dose response, regression analysis was performed using SigmaPlot v11.0 software (Systat Software, San Jose, CA, USA).

^{63}Ni microirradiator β-irradiation

A micromanipulator (World Precision Instruments, Sarasota, FL, USA) was mounted inside the WeatherStation environmental chamber of the Applied Precision Deltavision microscope to facilitate precise positioning of the microirradiator tip. The microirradiator probe was secured in an acrylic electrode holder. Cells were electroporated, incubated 24–48 h, transferred into the environmental chamber, and the microirradiator was positioned directly over a target cell, as determined by observation through the Deltavision optics. Time-lapse exposures were performed, with 15–24 Z-stack sections per timepoint, 0.4-μm section thickness, 0.5 s exposure time and auto-focusing in the EYFP channel. Images were deconvoluted, projection images were prepared and foci were scored manually. Foci present prior to irradiation were excluded.

To track and quantify individual foci, a region of interest was defined within the projection images, exported in TIF format, and loaded into DeCyder 6.5 software (GE Healthcare, Buckinghamshire, UK). Automated spot detection was performed, foci ('spots') were matched across the time-lapse images, and spot volumes were determined and plotted as a function of time.

RESULTS

Microscope stage-mounted irradiation system

The microirradiator was made by electrochemical deposition of an ~1-μm thick layer of ^{63}Ni on a 25 μm-diameter microelectrode wire enveloped in a glass capillary (5). The configuration of the device used here was similar to the 'recessed disk' design reported earlier (5), except that the device was prepared without etching the tip of the microelectrode, allowing ^{63}Ni to be plated directly onto a flush, polished Pt surface. This design change eliminates concern over attenuation of activity due to trapping of medium or debris in the cavity of the 'recessed disk' configuration. The isotopic enrichment of the ^{63}Ni was higher, resulting in a more highly active probe surface. In addition, a polymer PEDOT coating was applied to prevent direct contact between the Ni surface and the cell medium.

The microirradiator was mounted within the WeatherStation environmental chamber of an Applied Precision Deltavision microscope (Figure 1A), using a precision micromanipulator with an acrylic electrode holder (Figure 1B). The micromanipulator allows precise manual adjustment of the position along three orthogonal axes.

A bend was introduced in the capillary such that the capillary tip is coaxial with the optical path (Figure 1C). A dissecting microscope view showing the flush tip is shown in Figure 1D. The microirradiator was positioned so that the tip of the capillary was slightly above the target cell and was visible through the microscope optics (Figure 1E). The plane of the active surface is parallel to the plane of the culture dish.

Calibration of biological reporter system

The EYFP-53BP1 expression construct was as described in 'Materials and Methods' section (Figure 2A) and consists of an intrinsically fluorescent enhanced yellow fluorescent protein domain joined to full-length 53BP1. It is essentially identical to constructs used in previous live-cell imaging studies [e.g. (10–12)]. The U2OS 2-6-3 recipient cells (8) are derived from the U2OS osteosarcoma cell line, which has been widely used in prior studies of 53BP1 foci formation (11,13).

To calibrate the number of foci per unit dose of radiation in this system, cells were exposed to 0–3 Gy of ^{137}Cs radiation and imaged 25–30 min post-exposure, at which time the response has reached a maximum. H2B-diHcRed (9) was co-expressed as a registration marker (14). Live cell images were collected (Figure 2B) and nuclear foci were scored manually using 8–24 nuclei for each dose point (Figure 2C). Regression analysis indicated formation of 27.4 foci per nucleus per Gy. The slope of the 53BP1 dose response curves is 1.4-fold greater than reported in a prior live-cell imaging study (12). This is consistent with the fact that the hypertriploid U2OS cells contain about 1.5-fold more DNA per nucleus than the quasi-diploid HT1080 cells in the prior study and thus present a larger target for radiation damage.

Real-time observation of microirradiator-induced foci formation

Results of several microirradiator experiments are shown in Figure 3. Cells were electroporated with EYFP-53BP1 and H2B-diHcRed expression constructs. After 24–48 h, they were transferred to the stage of the Deltavision microscope, where they were maintained in growth medium in a humidified 5% CO_2 atmosphere at 37°C. The microirradiator was positioned above a target cell and image collection was initiated within 1 min (Figure 3A). Z-stack images were collected at 5 min intervals. The irradiator was withdrawn after the 16 min timepoint and cells were allowed to recover for a further 46 min. Images were deconvoluted, projections were prepared and foci were counted manually. Results for three individual cells are presented in Figure 3. In all three instances, foci appear with no discernible lag and increase to a maximum ~35 min after the probe was withdrawn and 50 min after the start of the experiment. The absolute number of foci varied between experiments, perhaps reflecting slight differences in the position of the probe. In order to pool the data from the three experiments, we normalized the data to the percent of maximum response in each experiment. We calculated the mean and SD to obtain the data in the rightmost panel of Figure 3B.
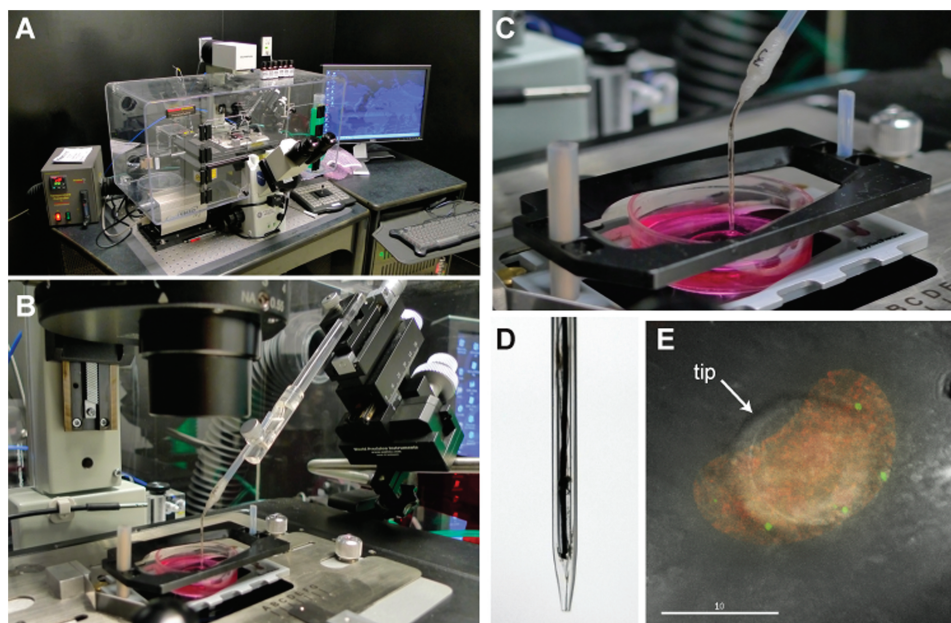
Figure 1. Microscope stage-mounted microirradiation system. (**A**) Gross view of microirradiation system. Device is mounted on a micromanipulator housed within a heated, humidified, environmental chamber of the Applied Precision Deltavision microscope. (**B**) Close-up view showing attachment of device to the micromanipulator. (**C**) Detail showing the bend in enclosing capillary, which allows positioning of the active surface directly above the target cell. (**D**) View of the microirradiator tip in dissecting microscope. (**E**) Close-up view through Deltavision microscope optics. Cell has been transfected with EYFP-53BP1 and H2B-diHcRed expression plasmids as described in 'Materials and Methods' section. Scale bar, 10 microns.
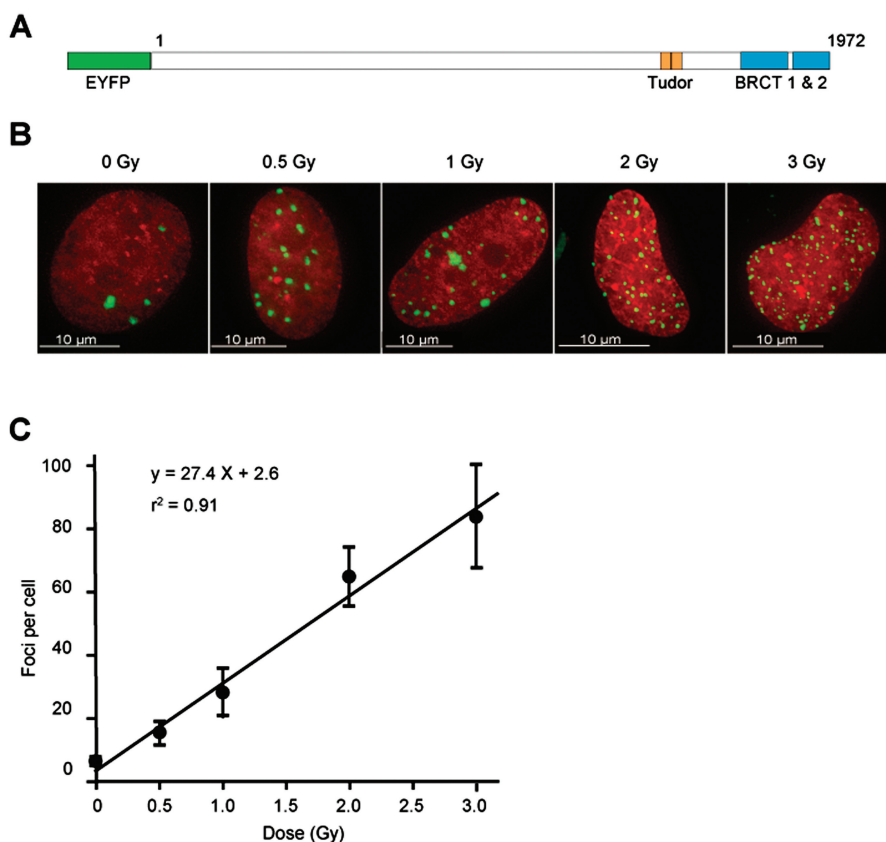

Figure 2. Calibration EYFP-53BP1 reporter system. (**A**) EYFP-53BP1 primary structures. EYFP coding sequence is joined to full-length 53BP1, with Tudor and BRCT domains indicated. EYFP1-53BP coding sequence was inserted into pcDNA-DEST40 (Invitrogen) for expression under control of the CMV promoter. (**B**) Dose response to calibrated doses of ^{137}Cs reference radiation. Cells were co-transfected with EYFP-53BP1 WT and H2B-diHcRed. Live-cell images were collected 30 min post-irradiation. (**C**) Quantification of dose response. Foci were scored using 8–24 individual nuclei at each dose point, and linear regression was performed to obtain the slope of the dose-response curve.
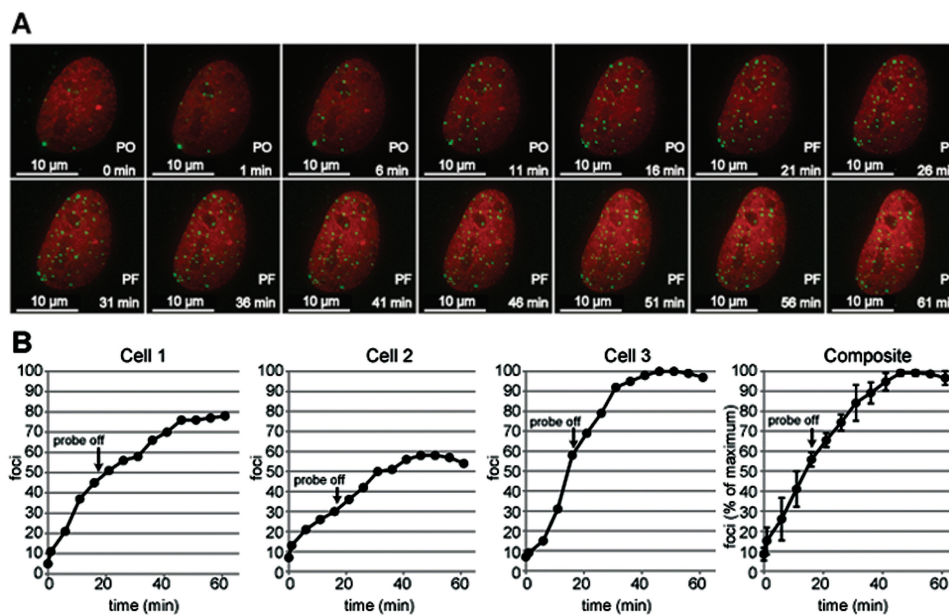
Figure 3. Real-time imaging of microirradiator-induced 53BP1 foci. (**A**) Representative images of same cell collected at indicated time points. Microirradiator was introduced 1 min prior to the first time point and withdrawn after the 16 min. Z-stacks containing 15–24 individual images were collected at each time point and deconvoluted. Projections are shown. PO, probe on; PF, probe off. (**B**) Quantification of microirradiator-induced foci from three independent experiments. Cell 1 corresponds to images in Panel A. Rightmost panel shows pooled data from the three experiments. Data were normalized to maximum response = 100%, averaged, and plotted. Error bars denote SD.

The result is a smooth curve showing an increase with approximately linear kinetics until a plateau is reached. No foci were seen in control cells imaged under the same conditions without the microirradiator (Supplementary Figure S1)

To estimate the radiation dose based on foci numbers to radiation dose, we compared the maximum number of foci attained in each experiment in Figure 3 to the calibration curves in Figure 2. We did not make an adjustment for the different radiation types (high energy γ rays versus β particles) as they may be considered as radiobiologically equivalent. We also did not adjust for dose rate. Because of this, the number of foci in Figure 3 may be slightly underestimated (i.e. a lower dose rate affords more time for the earliest foci to be resolved before the maximum is attained). Subject to these caveats, comparison with the standard curve indicates that the apparent dose delivered by the microirradiator in a 16 min exposure was 2.8, 2.0 and 3.6 Gy for cells 1, 2 and 3, respectively. The variability between cells could be due to differences in the intrinsic sensitivity of different cells (e.g. position in the cell cycle or, perhaps, to small differences in the positioning of the probes. These doses equate to dose rates range of 0.12–0.22 Gy/min. This is about an order of magnitude less than predicted by modeling a source with this activity and geometry ('Discussion' section), and the reason for the difference is still to be determined.

Although an effort was made to minimze the light exposure during imaging, we were aware of the possibility that phototoxicity might itself result in repair foci formation. We therefore performed a mock irradiation under the same conditions, but without the microirradiator.

No time-dependent accumulation of foci was seen above the background present at the beginning of the experiment (Supplementary Figure S1).

Dynamic behavior of individual foci

The time course in Figure 3B shows that the time between initial traversal of a radiation track and appearance of foci is variable, as some foci appeared immediately after the onset of irradiation, whereas others did not appear until 30 min after microirradiator was removed. It also follows from inspection of the shape of the curve that the time required for resolution of foci must also be variable. If the foci appeared at variable times post-exposure, but all were long-lived (i.e. persistent throughout the experiment), then a plot of foci versus time should be strongly sigmoidal. This was not the case. Instead, the system rapidly approached a steady state, showing a quasilinear response over the first 50 min. To account for this steady state, some of the foci that appear rapidly must also disappear rapidly.

To test this prediction, we tracked the behavior of individual foci over time. Figure 4A shows the same nuclei as in Figure 3A, but with expansion of a region of interest. Eighteen foci ('spots') were matched manually across the time series and intensities were quantified as described in 'Materials and Methods' section (refer also to Supplementary Figure S2). Figure 4B shows plots of spot volumes as a function of time. Several patterns are seen in these data. Foci 7, 9 and 11 appear and disappear rapidly, losing at least half their peak intensity within 10 min. Foci 1, 2, 5, 10, 12 and 15 decay with intermediate kinetics, losing half their peak intensity within 15–30 min.

Foci 3, 6, 14, 16, 17 and 18 were stable for the duration of the experiment. Foci 4, 8 and 13 showed somewhat irregular behavior.

Clearly, it will be of interest to collect longer and finer-grained time series, to analyze larger numbers of foci, and to perform a more computationally intensive analysis using the original 3D imaging data, rather than the 2D projections that were analyzed here. Even this limited analysis, however, suggests that foci fall into several classes, with some appearing and disappearing rapidly and others that are stable over the period of observation.

DISCUSSION

We describe here the first biological application of a novel microirradiator that is designed specifically for compatibility with a standard cell biology laboratory environment. The device is characterized by small physical dimensions, radiation flux sufficient for many types of biological experiments and minimal radiological hazards. We demonstrate the use of the device in experiments to track and characterize the induction of repair foci in irradiated cells. The microirradiator is a potential replacement for a self-contained $^{137}CsCl_2$ irradiator in certain cell and molecular biology research applications, particularly where biological response is measured at the single cell level. The device is made from inexpensive, commercially available materials, and the low total activity mitigates the public health and security concerns that have been raised for high-activity $^{37}CsCl_2$ radiation sources (3).

Because the microirradiator can be mounted directly to a microscope stage, it provides a capability for real-time observation of the early stages of the radiation response. This early response has not been well studied, particularly for sparsely radiation such as γ rays and X-rays. Preliminary analysis has revealed heterogeneous behavior of repair foci. In particular, there is a class of rapidly resolved foci that would not be apparent in experiments using conventional irradiation methods. The existence of a rapidly resolved subset of foci is significant because it may account for a small, but unexplained, discrepancy between the best estimate of the number of double strand breaks determined by physical methods ($\sim$30 DSBs per Gy per diploid genome) (15,16) and the number of breaks estimated by careful counting of ionizing radiation-induced foci ($\sim$10–25 foci per Gy per diploid genome) (6,12) reviewed in (1). Several explanations for the heterogeneous behavior of repair foci may be contemplated, including heterogeneity in the structure of the radiation-induced DNA breaks and the existence of competing repair or signaling pathways. Potentially, these explanations could be investigated by selective knockdown of individual DNA processing and repair enzymes in the target cells.

The present dose rate, estimated to be in the range of 0.12–0.22 Gy/min, is sufficient for many experiments to investigate the biology of the low-dose radiation response. A higher dose rate would be useful for experiments that require synchronous induction of large numbers of DSBs. The thickness of the nickel layer is sufficient that self-absorption is a limiting factor in controlling surface flux density, so that deposition of more radioisotope would not result in a corresponding increase in dose rate. The specific activity of the nickel-63 used here is the highest that is commercially available. However, the activity as stated by the vendor equates to <10% isotopic enrichment, so improvement is theoretically possible.

We have attempted to compare the dose rate estimated from the biological response to the predicted dose rate based on probe activity (as determined by liquid scintillation counting) and modeling as described in (5) (refer to Supplementary Data for details). A discrepancy between this predicted dose rate (2.65 Gy/min) and the estimated dose rate based on biological response suggests either that there is a flaw in the modeling or that the β emissions are attenuated in some unanticipated way. Further insight may be provided by experiments currently underway to characterize β particle flux and emission spectrum using solid-state scintillation counting (J.S. and J.J., unpublished data).

It is useful to compare the microirradiator to two other approaches that are currently in use to introduce targeted DNA damage into samples on a microscope stage. One of these is the particle microbeam. More than 50 years ago, Zirkle and Bloom (17) described the use of a Van de Graaf generator and microaperture to deliver an intense proton beam to a 2.5-μm diameter spot within living cells. It is now estimated that there are 30 operational microbeam facilities worldwide (18). Microbeam facilities have been developed that are capable of delivering precisely targeted heavy particles, electrons or ultrasoft X-ray photons, with varying degrees of real-time imaging capability [e.g. (19–23)]. As currently configured, the microirradiator lacks the capabilities for precision targeting and particle counting that are found at the most advanced microbeam facilities. The portability of the microirradiator and its potentially low cost of manufacture provide offsetting advantages, however, for many applications. Localized ultraviolet irradiation (or, equivalently, 2-photon absorption in the near infrared range) provides another approach that is useful in analysis of the DNA damage response [reviewed in (24), see also (25)]. The value of the approach is its ability to induce dense, near-instantaneous damage in a precisely localized region. This is also, however, its main limitation, as the dense DNA damage has no clear physiological equivalent, whereas the low-energy β particles from the nickel-63 microirradiator are expected to produce damage that is similar in type and distribution to that from common medical and environmental exposure sources. Thus, the characteristics of the Ni-63 microirradiator make it a useful complement to other technologies that are currently in use.

In principle, it should be possible to adapt the same electroplating technology to construct analogous microirradiators using other radioisotopes. For example, ^{252}Cf could be used as a source of fission neutrons or ^{241}Am as a source of α particles. Both of these isotopes are used industrially and are potentially available for construction of research microirradiators. The cellular and
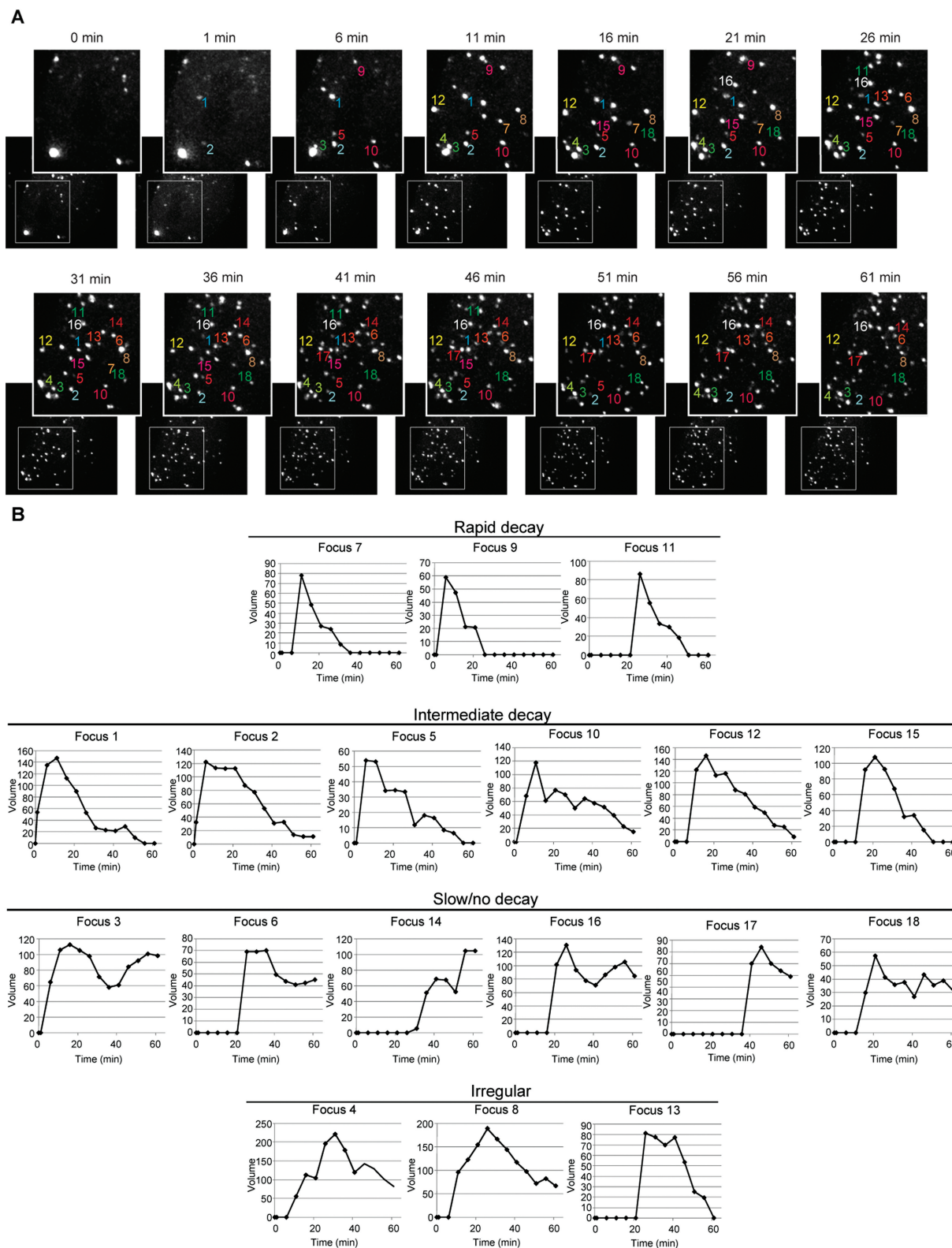
Figure 4. Tracking of individual 53BP1 foci. (**A**) Images are from nuclei from Cell 1 in Figure 3. Inset panels show enlargement of region of interest marked by white rectangle. Eighteen individual foci were identified manually and are marked. (**B**) Quantification of image intensity for individual foci. The 2D image projections were loaded in DeCyder v6.5 (GE Healthcare, Buckinghamshire, UK) and automated spot detection was performed (Supplementary Figure S2). Volumes corresponding to integrated signals for each spot were quantified. Plots show image intensity for individual foci as a function of time. The same arbitrary units are used in all panels. Time is indicated in min.

molecular response to high LET radiation, such as neutrons and α particles, has not been as extensively studied as low LET radiation, in part because convenient sources are not available outside the radiation community. Concentrated deposition of isotope on a very small surface in the microirradiator allows experiments to be performed using very small total amount of isotope, mitigating health and safety concerns that pose barriers to access to nuclear materials.

SUPPLEMENTARY DATA

Supplementary Data are available at NAR Online.

ACKNOWLEDGEMENTS

FUNDING

REFERENCES

1. Kinner,A., Wu,W., Staudt,C. and Iliakis,G. (2008) Gamma-H2AX in recognition and signaling of DNA double-strand breaks in the context of chromatin. *Nucleic Acids Res.*, **36**, 5678–5694.
2. Pandita,T.K. and Richardson,C. (2009) Chromatin remodeling finds its place in the DNA double-strand break response. *Nucleic Acids Res.*, **37**, 1363–1377.
3. *Radiation Source Use and Replacement: Abbreviated Version* (2008). National Academies Press, Washington, D.C.
4. Munro,T.R. (1958) Alpha irradiation of parts of single cells in tissue cultures. *Exp. Cell. Res.*, **15**, 529–550.
5. Steeb,J., Josowicz,M. and Janata,J. (2009) Nickel-63 Microirradiators. *Anal. Chem.*, **81**, 1976–1981.
6. Costes,S.V., Chiolo,I., Pluth,J.M., Barcellos-Hoff,M.H. and Jakob,B. (2010) Spatiotemporal characterization of ionizing radiation induced DNA damage foci and their relation to chromatin organization. *Mutat. Res.*, [8 January 2010, Epub ahead of print].
7. FitzGerald,J.E., Grenon,M. and Lowndes,N.F. (2009) 53BP1: function and mechanisms of focal recruitment. *Biochem. Soc. Trans.*, **37**, 897–904.
8. Kumaran,R.I. and Spector,D.L. (2008) A genetic locus targeted to the nuclear periphery in living cells maintains its transcriptional competence. *J. Cell. Biol.*, **180**, 51–65.
9. Gerlich,D., Beaudouin,J., Kalbfuss,B., Daigle,N., Eils,R. and Ellenberg,J. (2003) Global chromosome positions are transmitted through mitosis in mammalian cells. *Cell*, **112**, 751–764.
10. Pryde,F., Khalili,S., Robertson,K., Selfridge,J., Ritchie,A.M., Melton,D.W., Jullien,D. and Adachi,Y. (2005) 53BP1 exchanges slowly at the sites of DNA damage and appears to require RNA for its association with chromatin. *J. Cell. Sci.*, **118**, 2043–2055.
11. Jakob,B., Splinter,J., Durante,M. and Taucher-Scholz,G. (2009) Live cell microscopy analysis of radiation-induced DNA double-strand break motion. *Proc. Natl. Acad. Sci. USA*, **106**, 3172–3177.
12. Asaithamby,A. and Chen,D.J. (2009) Cellular responses to DNA double-strand breaks after low-dose gamma-irradiation. *Nucleic Acids Res.*, **37**, 3912–3923.
13. Schultz,L.B., Chehab,N.H., Malikzay,A. and Halazonetis,T.D. (2000) p53 binding protein 1 (53BP1) is an early participant in the cellular response to DNA double-strand breaks. *J. Cell. Biol.*, **151**, 1381–1390.
14. Rabut,G. and Ellenberg,J. (2004) Automatic real-time three-dimensional cell tracking by fluorescence microscopy. *J. Microsc.*, **216**, 131–137.
15. Ruiz de Almodovar,J.M., Steel,G.G., Whitaker,S.J. and McMillan,T.J. (1994) A comparison of methods for calculating DNA double-strand break induction frequency in mammalian cells by pulsed-field gel electrophoresis. *Int. J. Radiat. Biol.*, **65**, 641–649.
16. Iliakis,G.E., Cicilioni,O. and Metzger,L. (1991) Measurement of DNA double-strand breaks in CHO cells at various stages of the cell cycle using pulsed field gel electrophoresis: calibration by means of 125I decay. *Int. J. Radiat. Biol.*, **59**, 343–357.
17. Zirkle,R.E. and Bloom,W. (1953) Irradiation of parts of individual cells. *Science*, **117**, 487–493.
18. Gerardi,S. (2009) Ionizing radiation microbeam facilities for radiobiological studies in Europe. *J. Radiat. Res.*, **50(Suppl. A)**, A13–A20.
19. Randers-Pehrson,G., Geard,C.R., Johnson,G., Elliston,C.D. and Brenner,D.J. (2001) The Columbia University single-ion microbeam. *Radiat. Res.*, **156**, 210–214.
20. Gerardi,S. (2006) A comparative review of charged particle microbeam facilities. *Radiat. Prot. Dosimetry.*, **122**, 285–291.
21. Folkard,M., Schettino,G., Vojnovic,B., Gilchrist,S., Michette,A.G., Pfauntsch,S.J., Prise,K.M. and Michael,B.D. (2001) A focused ultrasoft x-ray microbeam for targeting cells individually with submicrometer accuracy. *Radiat. Res.*, **156**, 796–804.
22. Kim,E.H., Sun,G.M. and Jang,M. (2006) An electron microbeam cell-irradiation system at KIRAMS: performance and preliminary experiments. *Radiat. Prot. Dosimetry*, **122**, 297–300.
23. Sowa,M.B., Murphy,M.K., Miller,J.H., McDonald,J.C., Strom,D.J. and Kimmel,G.A. (2005) A variable-energy electron microbeam: a unique modality for targeted low-LET radiation. *Radiat. Res.*, **164**, 695–700.
24. Kong,X., Mohanty,S.K., Stephens,J., Heale,J.T., Gomez-Godinez,V., Shi,L.Z., Kim,J.S., Yokomori,K. and Berns,M.W. (2009) Comparative analysis of different laser systems to study cellular responses to DNA damage in mammalian cells. *Nucleic Acids Res.*, **37**, e68.
25. Suzuki,K., Yamauchi,M., Oka,Y., Suzuki,M. and Yamashita,S. (2010) A novel and simple micro-irradiation technique for creating localized DNA double-strand breaks. *Nucleic Acids Res.*, [12 April 2010, Epub ahead of print].